Biocompatible Reinforcement of Poly(Lactic Acid) With Graphene Nanoplatelets

Carolina Gonçalves, [1] Artur Pinto, [2,3,4] Ana Vera Machado, [5] Joaquim Moreira, [6] Inês C. Gonçalves, [3,4] Fernão Magalhães [2]

[1] ARCP - Competence Network in Polymers Association, Inovation Center - UPTEC, Rua do Dr. Júlio de Matos 828/882, 4200-355 Porto, Portugal

[2] LEPABE - Laboratory for Process Engineering, Environmental, Biotechnology and Energy, Faculty of Engineering, University of Porto, Rua Dr. Roberto Frias, 4200-465 Porto, Portugal

[3] i3S - Institute for Research and Innovation in Health, University of Porto, Rua Alfredo Allen, 208, 4200-135 Porto, Portugal

[4] INEB - National Institute of Biomedical Engineering, University of Porto, Rua Alfredo Allen, 208, 4200-135 Porto, Portugal

[5] Institute of Polymers and Composites/I3N, University of Minho, 4800-058 Guimarães, Portugal

[6] IFIMUP and IN - Institute of Nanoscience and Nanotechnology, University Department of Physics and Astronomy, Faculty of Sciences, University of Porto, Rua do Campo Alegre 687, 4169-007 Porto, Portugal

A recently made available form of graphene nanoplatelets (GNP-C) is investigated for the first time as reinforcement filler for PLA. GNP-C, with thickness of about 2 nm and length $1-2\mu$ m, was incorporated at different loadings (0.1-0.5 wt%) in poly(lactic acid) (PLA) by melt blending. The effect of varying mixing time and mixing intensity was studied and the best conditions were identified, corresponding to mixing for 20 min at 50 rpm and 180°C. Thermal analysis (differential scanning calorimetry and thermogravimetric analysis) indicated no relevant differences between pristine PLA and the composites. However, the rate of thermal degradation increased with loading, due to the dominant effect of heat transfer enhancement over mass transfer hindrance. Raman spectroscopy allowed confirming that increasing graphene loading or decreasing mixing time translates into higher nanoplatelet agglomeration, in agreement with the observed mechanical performance and scanning electron microscopy imaging of the composites. The composites exhibited maximum mechanical performance at a loading of 0.25wt% : 20% increase in tensile strength, 12% increase in Young's modulus, and 16% increase in toughness. The incorporation of 0.25wt% GNP-C did not affect human fibroblasts (HFF1) metabolic activity or morphology.

INTRODUCTION

In the last two decades, polymer composites have been studied as a strategy to provide added value properties to neat polymer without sacrificing its processability or adding excessive weight. Particular attention has been given to reinforcement with nanosized materials, which have the potential to present improved or even new properties when compared to conventional filled polymers [1].

Poly(lactic acid) (PLA) has great worldwide demand due to versatile applicability in packaging, pharmaceutical, textiles, automotive, biomedical, and tissue engineering [2]. It has been widely investigated for biomedical applications due to its biodegradability, bioresorbability, and biocompatibility [3, 4]. Several applications have been described in tissue and surgical implant engineering, for production of bioresorbable artificial ligaments, hernia repair meshes, scaffolds, screws, surgical plates, and suture yarns [5]. PLA is also used in production of nano/microcapsules for drug delivery, and in packaging of pharmaceutical products [6]. Improvement and tuning of its properties has been reported by incorporation of plasticizers, blending with other polymers, and addition of nanofillers [7-9].

Carbon-based fillers offer the potential to combine several unique properties, such as mechanical strength, electrical conductivity, thermal stability, and physical and optical properties, required for a spectrum of applications [10-12]. Graphene, in particular, has been playing a key role in modern science and technology. Its remarkable properties and the natural abundance of its precursor, graphite, make it an interesting option for production of functional composites [13]. Graphene is a one-atom-thick planar sheet of sp^2-bonded carbon atoms densely packed in a honeycomb crystal lattice. It possesses very high mechanical strength, surface area per unit mass, and thermal and electrical conductivities. In the last years, there has been a surge in research work involving this material, with reported applications in diverse fields, including biomedical engineering and biotechnology [14-20]. On the other hand, not many studies are yet available concerning biocompatibility of graphene and graphene-based materials (GBM). These often show contradictory results [21-26]. In our recent study, graphene nanoplatelets with smaller size (GNP-C) revealed to be biocompatible with human fibroblasts (HFF-1) until a concentration of $50\mu\,g\,mL^{-1}$, opposing to larger GNP-M, which are toxic above $20\mu\,g\,mL^{-1}$ [27]. Since several authors have shown that effective reinforcement of polymeric matrices can be obtained with small loadings of GBM [28-32], toxic concentrations achievement can be prevented. Additionally, graphene oxide (GO) and graphene nanoplatelets (GNP), grade M (GNP-M), have shown not to affect mouse embryo fibroblasts metabolic activity when incorporated in PLA at a loading of 0.4wt% [33].

Many graphene-related materials have been reported in literature as potentially interesting fillers for polymer reinforcement. One commercial product that has been receiving particular attention, and is the object of study in this paper, is GNP: stacks of few graphene layers obtained by rapid heating of intercalated graphite. The platelets surface consists of mostly defect-free graphene, while oxygen is present in the sheet edges, in the form of, for instance, hydroxyl or carboxyl groups. Even though different grades are available for this material, grade M, with average platelet thickness of $6-8$ nm and maximum length of 5μ m, is the most often tested in the available literature [31].

Several studies exist on reinforcement of PLA with GBM. Even though performance improvements are reported, quantitative results are usually distinct, owing mainly to differences in chemical and morphological nature of GBM, filler incorporation and processing methods, and filler loadings. Cao et al. observed an 18% increase in Young's modulus with addition of only 0.2wt% of reduced graphene oxide [30]. The composite was prepared by solution mixing, followed by flocculation and drying. Pinto et al. showed that small loadings of GO and GNP-M (0.4 wt%) in PLA thin films produced by solvent evaporation significantly improved mechanical and gas permeation barrier properties [31]. Tensile strength and Young's modulus were increased by about 15% and 85%, respectively. Chieng et al. investigated PLA/PEG melt blends with GNP-M loadings of 0.3wt%, obtaining increases of 33%, 69%, and 22% in tensile strength, Young's modulus, and elongation at break [34]. Bao et al. prepared PLA/graphene composites by melt blending and observed 58% improvement in storage modulus at 0.2wt% loading [35]. Yang et al. prepared poly(Llactic acid) (PLLA)/thermally reduced graphene oxide composites via in situ ring-opening polymerization of lactide. The composite materials obtained, with loadings up to 2wt%, showed improved thermal stability, electrical conductivity, and crystallization rate [36]. In the work of Kim and Jeong, exfoliated graphite was incorporated in PLLA at different loadings by melt blending [37]. At 2wt% loading, tensile strength increased by about 13% and Young's modulus by 33%. Wenxiao et al. studied PLLA composites containing different low-dimensional carbonaceous fillers, with constant filler content of 0.5wt%. The fillers were pristine and silanized multiwalled carbon nanotubes (MWNTs) and exfoliated graphene [38]. All composites were prepared by solution mixing. It was found that tensile strength, elongation at break, and Young's modulus showed similar improvements when using carbon nanotubes or graphene (about 20%, 39%, and 33%, respectively). Silane modification of both fillers further improved elongation at break and Young's modulus, without sacrificing tensile strength. More recently, Wenxiao et al. successfully grafted GO with PLLA by in situ polycondensation [39]. This material was incorporated in PLLA by solution mixing, and the composite with 0.5wt% loading showed improvements in flexural and tensile strengths of 114% and 106%, respectively.

In this study, a recently made available commercial grade of GNP (grade C), made of thinner and shorter platelets than existing grades, is investigated for the first time as reinforcement filler for PLA. Melt blending is used for preparing the composite material as this is an economically attractive and industrially scalable method for efficiently dispersing nanofillers in thermoplastic polymers. The effects of blending conditions (mixing time, intensity, and temperature) and filler loading on the composite properties are analyzed, and the best conditions identified. This is an important aspect since results are often dependent on processing conditions, and this type of analysis is often absent from the literature. Melt blending is an environmentally friendly method for filler incorporation that does not involve use of solvents. It avoids concerns with human health during processing and with toxicity of remaining solvent residues.

The quality of filler dispersion in the PLA matrix is investigated by SEM and Raman spectroscopy, and is seen

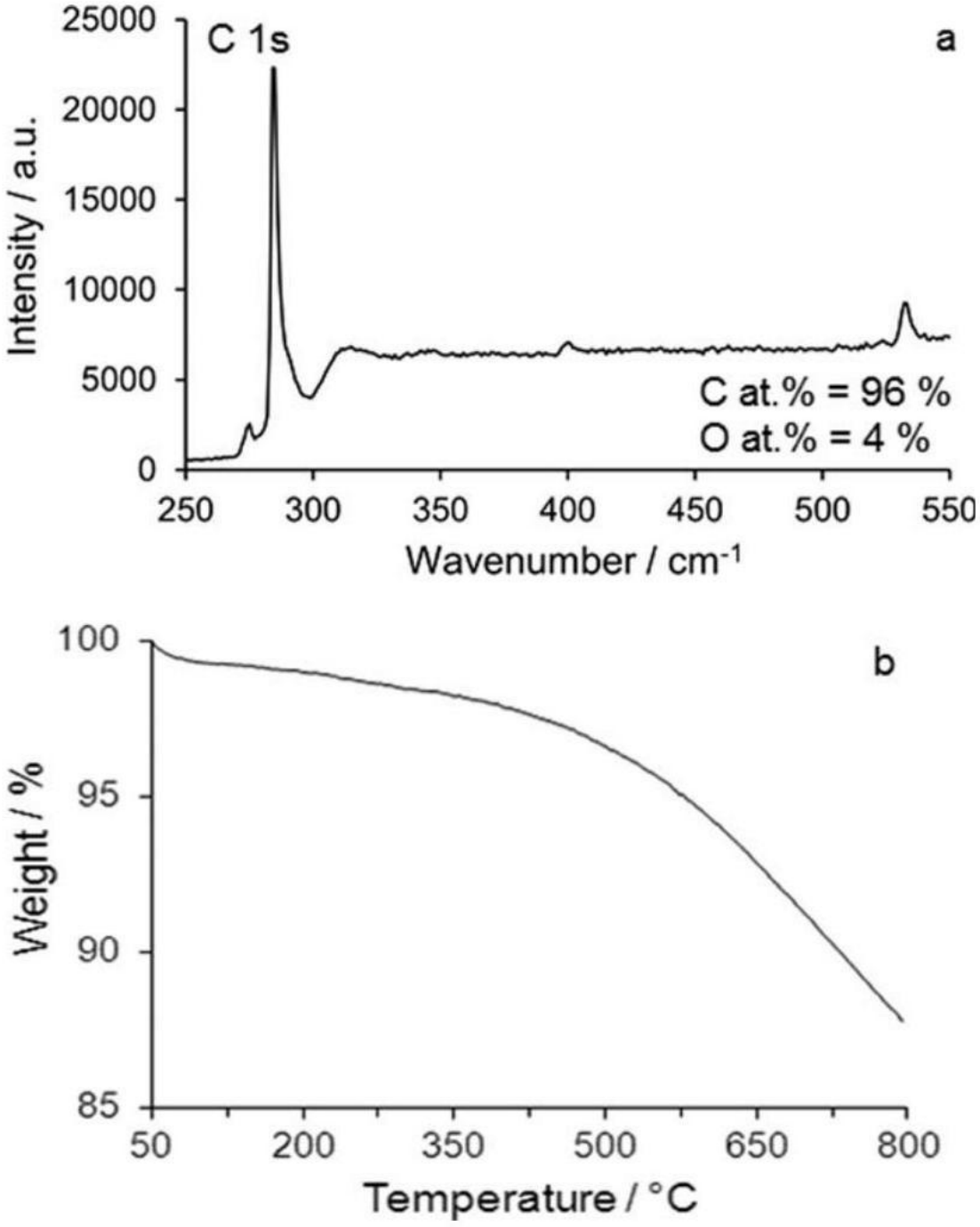

FIG. 1. (a) XPS spectrum for atomic composition of GNP-C powder; (b) TGA curve for GNP-C powder.

to have a major influence on mechanical properties. For the first time, the biocompatibility of PLA/GNP-C composites is studied, namely, in terms of effects on cell metabolic activity and morphology.

EXPERIMENTAL

Materials

Poly(lactic acid) (PLA) 2003D (4% d-lactide, 96% Llactide content) was purchased from Natureworks (Minnetonka, USA).

GNP, grade C750 (GNP-C), was acquired from XG Sciences (Lansing, USA), with the following characteristics, according to the manufacturer: average thickness lower than

2 nm and surface area of 750 $m^2\ g^{-1}$. The platelet diameters have a distribution that ranges from tenths of micrometer up to $1-2\mu$ m. GNP production is based on exfoliation of sulphuric acid-based intercalated graphite by rapid microwave heating, followed by ultrasonic treatment [64].

Preparation of PLA/GNP Composites

The PLA/GNP composites were prepared by melt blending in a Thermo Haake Polylab internal mixer (internal mixing volume 60 cm^3) at different temperatures (180,200, 225 , and 250°C) mixing times (10,15 , and 20 min) and rotor speeds (25,50 , and 75 rpm). The GNP contents tested were 0.1,0.25, and 0.5wt%. After removal from the mixer, the composites were molded in a hot press at 190°C for 2 min, under a pressure of 150 kg/cm^2, into sheets with approximately 0.5 mm thickness. After pressing, the sheets were rapidly cooled in water at room temperature. Samples with different dimensions were cut from these sheets, depending on the characterization test.

X-ray Photoelectron Spectroscopy (XPS)

GNP-C powder was analyzed with an Escalab 200 VG Scientific spectrometer working in ultrahigh vacuum (1×10^{-6} Pa) and using achromatic Al$K\alpha$ radiation (1486.6eV). The analyzer pass energy was 50 eV for survey spectra and 20 eV for high-resolution spectra. The spectrometer was calibrated using (Au3 d5/2 at 368.27 eV). The core levels for O 1s and C 1s were analyzed. The photoelectron takeoff angle (the angle between the surface of the sample and the axis of the energy analyzer) was 90°. The electron gun focused on the specimen in an area close to 100 mm^2.

Fourier Transform Infrared Spectroscopy (FTIR)

PLA and PLA/GNP-C FTIR spectra were obtained between 600 and 4000 cm^{-1}, with 100 scans and a resolution of 4 cm^{-1}, using a spectrometer ABB MB3000 (ABB, Switzerland) equipped with a deuterated triglycine sulphate detector and using a MIRacle single reflection horizontal attenuated total reflectance (ATR) accessory (PIKE Technologies, USA) with a diamond/Se crystal plate.

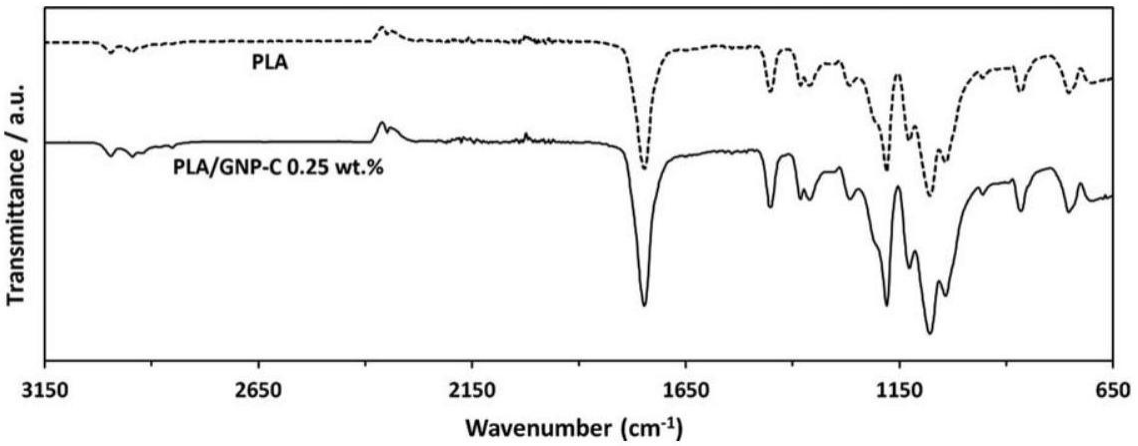

FIG. 2. FTIR spectra for PLA and PLA/GNP-C 0.25wt%(180°C, 20 min, and 50 rpm).

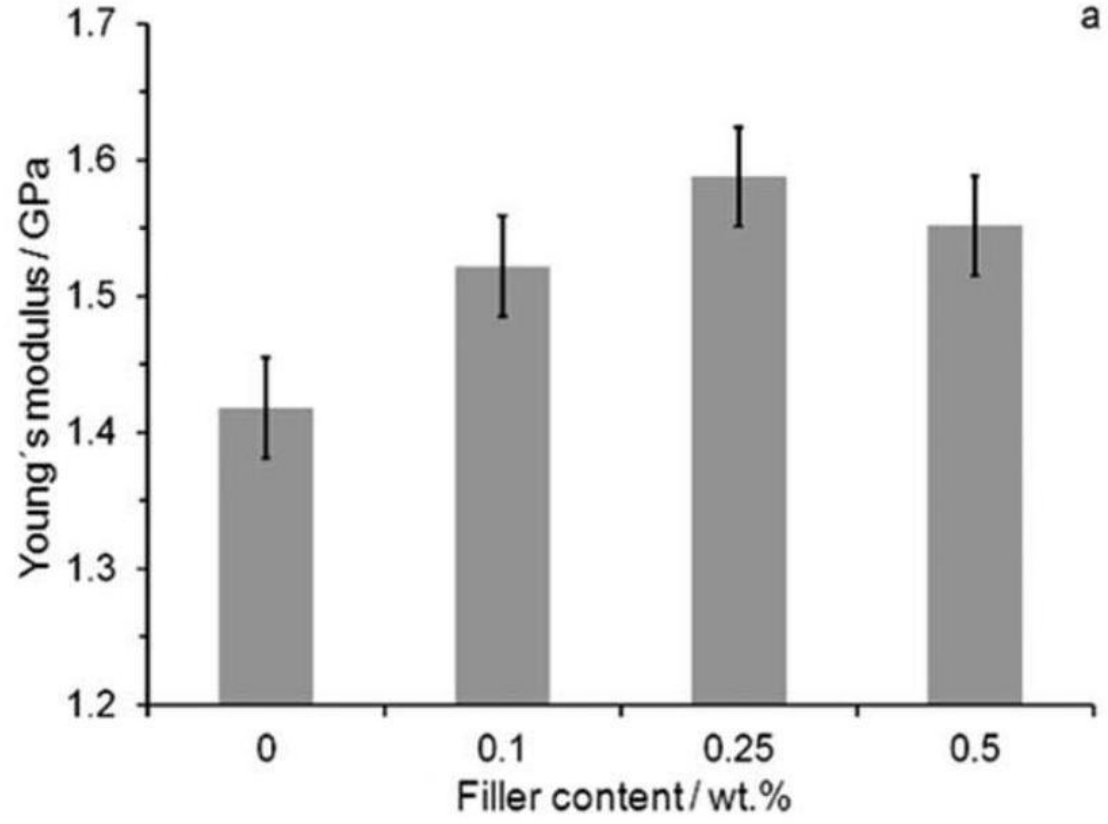
a
1.7
1.6
1.5
1.4
1.3
1.2
Young´s modulus / GPa
0
0.1
0.25
0.5
Filler content / wt.%

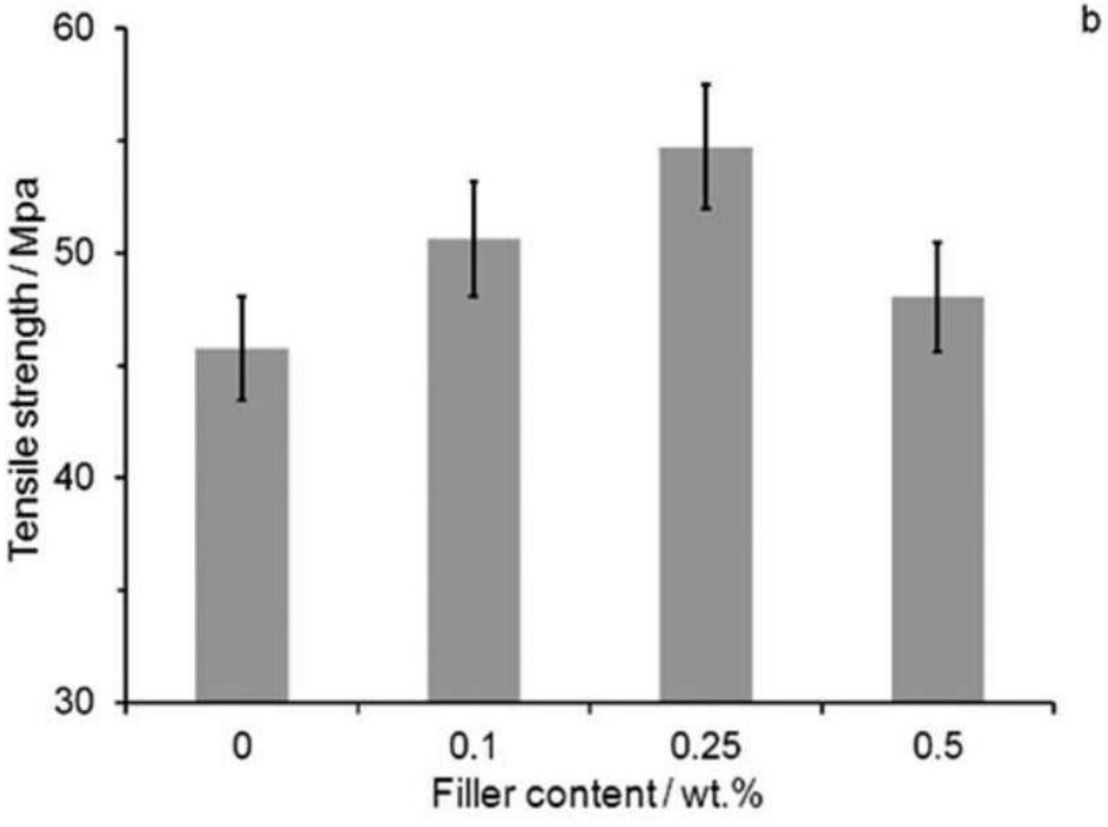
b
60
50
40
30
Tensile strength / Mpa
0
0.1
0.25
0.5
Filler content / wt.%

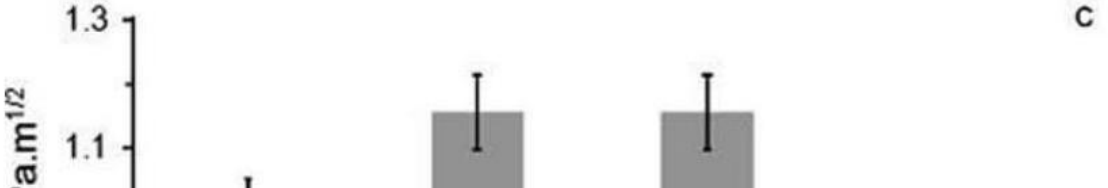
c
1.3
1.1

FIG. 3. Effect of increasing nanofiller content on mechanical properties of PLA/GNP-C composites under the same processing conditions ($180^{\circ}\mathrm{C}, 20$ min, and 50 rpm) : (a) Young's modulus; (b) tensile strength; (c) toughness. Error bars represent standard deviations computed from measurements on at least 10 samples.

Tensile Properties

Tensile properties of the composites (dimensions of 60×15 mm, thickness of $300 - 500\mu$ m) were measured using a Mecmesin Multitest-1d motorized test frame, at room temperature. Loadings were recorded with a Mecmesin BF 1000N digital dynamometer at a strain rate of 10 mm min^{-1}. The test parameters were in agreement with ASTM D 882-02. At least 10 samples were tested for each composite.

Glass transition temperatures (T_{g}) and melting temperatures (T_{m}) of samples were determined with a Setaram DSC 131 device. The thermograms were recorded between 30 and $200^{\circ}\mathrm{C}$ at a heating range of $10^{\circ}\mathrm{Cmin}^{-1}$ under nitrogen flow. Only the second heating thermograms were collected. Sample amounts ranged from 10 to 12 mg .

Thermal stability of samples was determined with a Netzsh STA 449 F3 Jupiter simultaneous thermal analysis device. Sample amounts ranged from 10 to 12 mg . The thermograms were recorded between 25 and $800^{\circ}\mathrm{C}$ at a heating rate of $10^{\circ}\mathrm{Cmin}^{-1}$ under nitrogen flow.

The degree of crystallinity was determined as follows: $\chi c(\%) = 100 \times \frac{(\mathrm{J}\Delta Hc + \mathrm{J}\Delta Hm)}{\mathrm{J}\Delta H_m^c}$, where ΔH_{c} is the cold crystallization enthalpy, ΔH_{m} is the melting enthalpy, and $\Delta H_{\mathrm{m}}^{\mathrm{c}}$ is the melting enthalpy of purely crystalline poly(L-lactide) [65].

Scanning Electron Microscopy (SEM)

The morphology of the PLA/GNP composites was observed using SEM (FEI Quanta 400FEG, with acceleration voltage of 3 kV) at Centro de Materiais da Universidade do Porto. Composites selected for SEM analysis were fractured transversely under liquid nitrogen, applied on carbon tape, and sputtered with Au/Pa (10 nm film). The number of agglomerates per unit of area (mm^2) as a function of agglomerate length, for different GNP-C loadings, was evaluated by direct measurements from 5 SEM images collected for each material, using ImageJ 1.45 software.

Raman Spectroscopy

The unpolarized Raman spectra of GNP-C powder, PLA, and PLA/GNP-C composites were obtained under ambient conditions, in several positions for each sample. The linear polarized 514.5 nm line of an Ar^{+}laser was used as excitation. The Raman spectra were recorded in a backscattering geometry by using a confocal Olympus BH-2 microscope with a $50 \times$ objective in a volume of $10\mu\ \mathrm{m}^3$. The spatial resolution is about 2μ m. The laser power was kept below 15 mW on the sample to avoid heating. The scattered radiation was analyzed using a Jobin-Yvon T64000 triple spectrometer, equipped with a charge-coupled device. The spectral resolution was better than 4 cm^{-1}.

The spectra were quantitatively analyzed by fitting a sum of damped oscillator to the experimental data, according to the equation [66]:

$$I(\omega,T) = (1 + n[\omega,T]) \sum_{j=1}^{N} A_{0j} \frac{\omega \Omega_{0j}^2 \Gamma_{0j}}{\left(\Omega_{0j}^2 - \omega^2\right)^2 + \omega^2 \Gamma_{0j}^2} \quad (1)$$

Here $n(\omega,T)$ is the Bose-Einstein factor: A_{0j}, Ω_{0j}, and Γ_{0j} are the strength, wave number, and damping coefficient

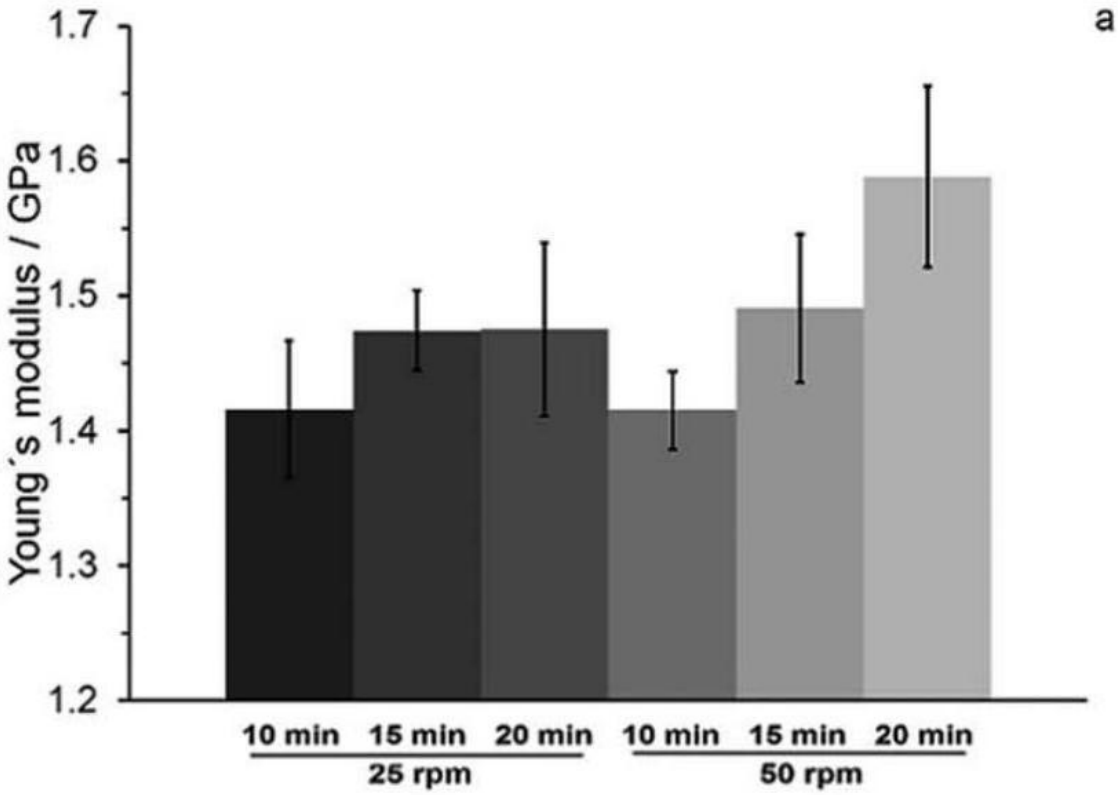
a
Young´s modulus / GPa
1.7
1.6
1.5
1.4
1.3
1.2
10 min
15 min
20 min
10 min
15 min
20 min
25 rpm
50 rpm

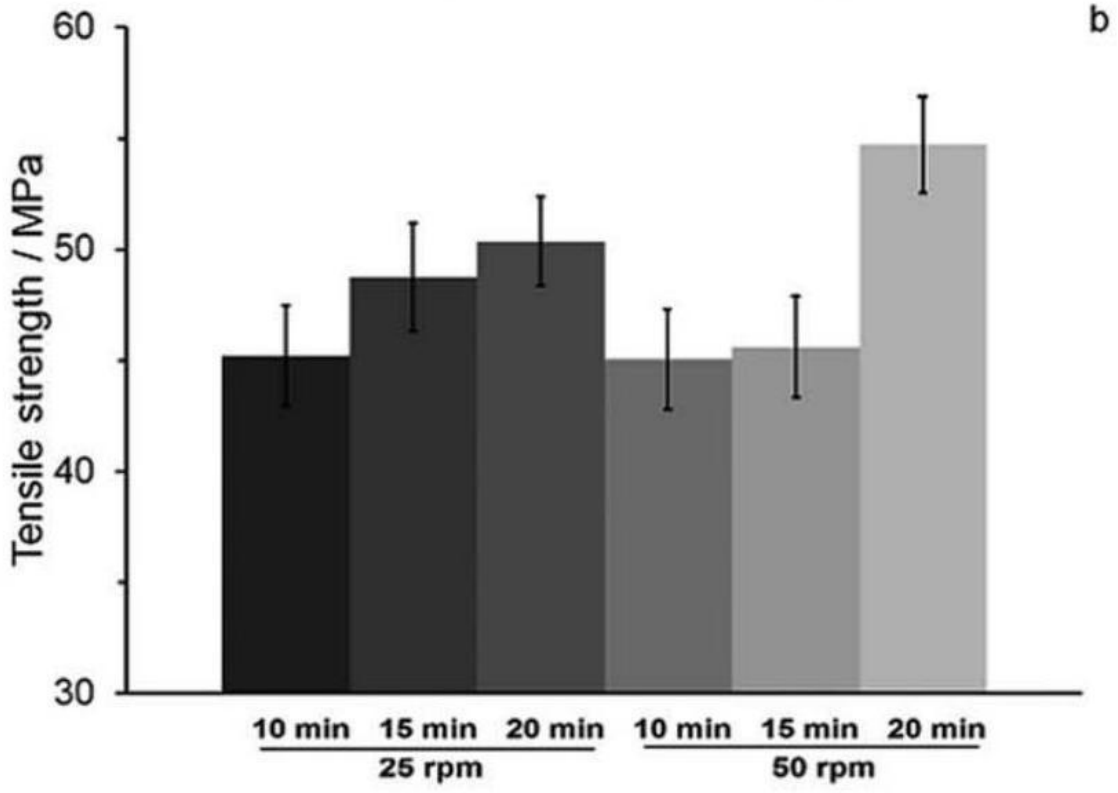
b
Tensile strength / MPa
60
50
40
30
10 min
15 min
20 min
10 min
15 min
20 min
25 rpm
50 rpm

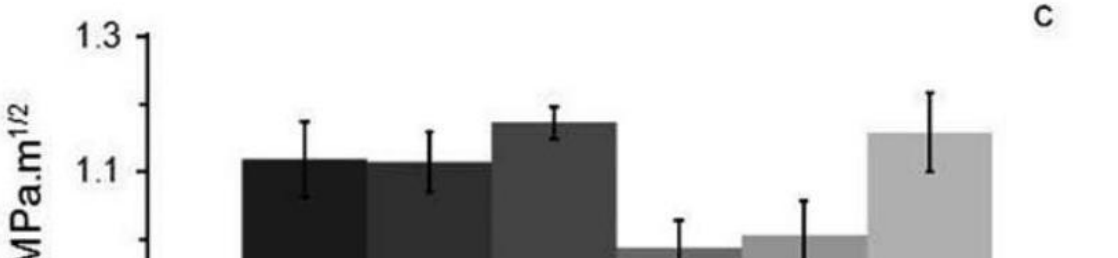
c
MPa.m1/2
1.3
1.1

FIG. 4. Effect of mixing time and rotation speed on mechanical properties of PLA/GNP-C composites processed at 180°C, for a filler content of 0.25wt% : (a) Young's modulus; (b) tensile strength; (c) toughness. Error bars represent standard deviations computed from measurements on at least 10 samples.
of the j th oscillator, respectively. In this work, the background was well simulated by a linear function of the frequency, which enables us to obtain reliable fits of Eq. 1 to the experimental data.

The fitting procedure was performed for all Raman bands collected from the same sample, but in different positions. This procedure allows us to determine the average and standard deviation (SD) values of the phonon parameters, namely, the wave number and intensity.

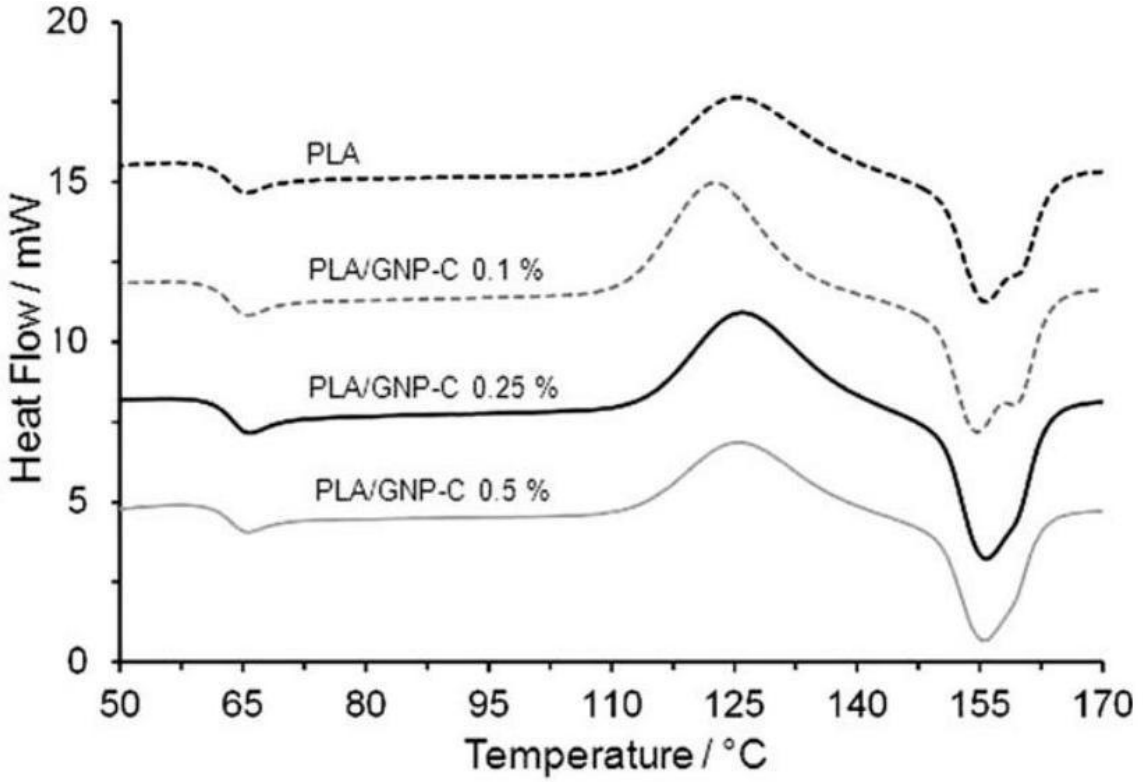

FIG. 5. DSC thermograms for PLA and PLA/GNP-C (180°C, 20 min, and 50 rpm) composites with different filler contents.

Biocompatibility Assays

Human foreskin fibroblasts HFF-1 (from ATCC) were grown in DMEM+ (Dulbecco's modified Eagle's medium (DMEM, Gibco) supplemented with 10% (V/V) newborn calf serum (Gibco) and 1% (V/V) penicillin/ streptomycin (biowest) at 37°C, in a fully humidified air containing 5%CO_2. The media were replenished every 3 days. When reaching 90% confluence, cells were rinsed with PBS (37°C) and detached from culture flasks ($TPP^{(R)}$) using 0.25% (w/V) trypsin solution (Sigma Aldrich) in PBS. All experiments were performed using cells between passages 10-14. Biocompatibility of the materials was evaluated using HFF-1 cells cultured at the surface of PLA and PLA/GNP-C

0.25wt% films ($\emptyset = 5.5$ mm). Cells were seeded at a density of 2×10^4 cells mL^{-1}. Resazurin (20μL) solution was added at 24,48 , and 72 h and incubated for 3 h , fluorescence ($\lambda_{\mathrm{ex/em}} = 530/590$ nm) read and metabolic activity evaluated (metabolic activity (%) $= F_{\mathrm{sample}}/F_{\mathrm{PLA}} \times 100$). All assays were performed in sextuplicate and repeated 3 times. Cell morphology was evaluated by immunocytochemistry at 72 h . Cells were washed with PBS and fixation was performed with paraformaldehyde (PFA, Merck) 4wt% in PBS for 15 min . PFA was removed, cells were washed with PBS, and stored at 4°C. Cell membrane was permeabilized with Triton X-100 0.1wt% at 4°C for 5 min . Washing was performed with PBS and incubation performed with phalloidin (Alexa Fluor 488; Molecular Probes) solution in

TABLE 1. Glass transition temperature (T_{g}) and melting temperature (T_{m}) for PLA and PLA/GNP-C composites (180°C, 20 min, and 50 rpm) with different filler contents

Samples (wt%)	T_{g} (°C)	T_{m} (°C)	T_{c} (°C)	ΔH_{c} (J/g)	ΔH_{m} (J/g)	X_{c} (%)
PLA	63.2	155.7	125.4	25.3	22.0	3.57
GNP-C 0.10	63.6	155.5	126.0	25.4	22.1	3.50
GNP-C 0.25	63.4	154.8	122.5	28.2	22.1	6.42
GNP-C 0.50	63.6	155.9	126.1	26.0	21.6	4.75

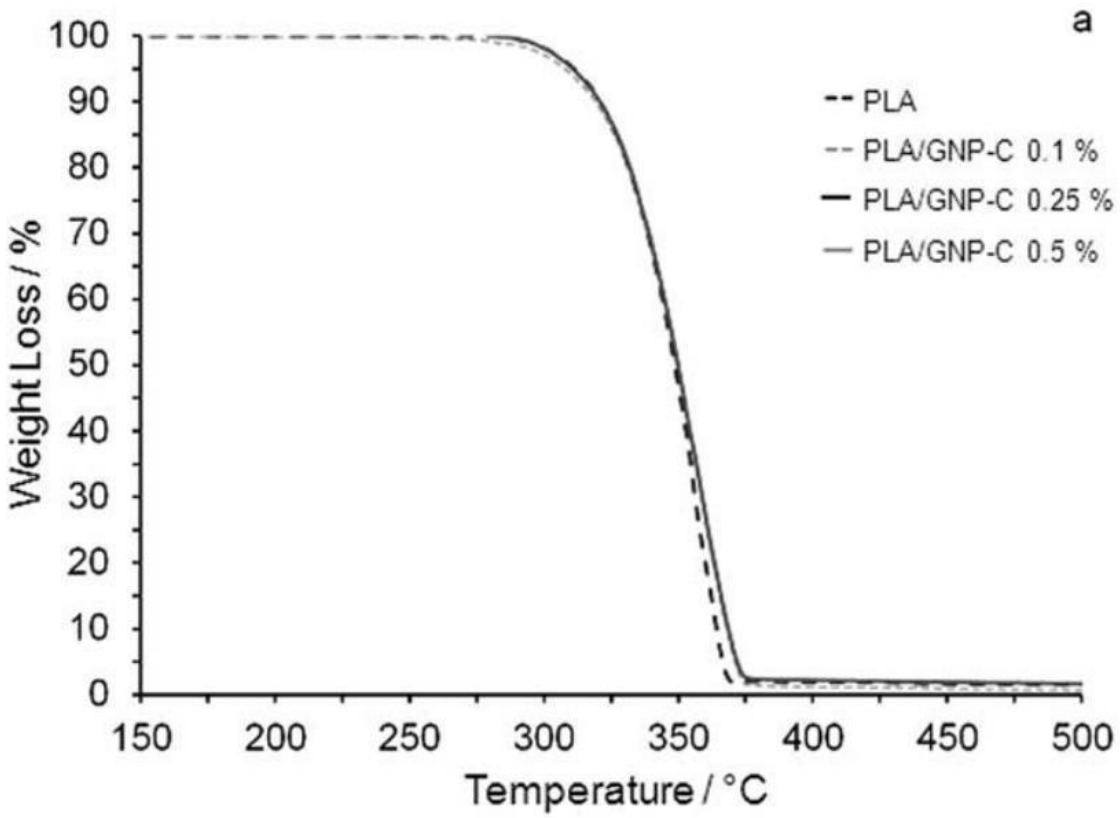
a
100
90
80
70
60
50
40
30
20
10
0
Weight Loss / %
150
200
250
300
350
400
450
500
Temperature / °C
PLA
PLA/GNP-C 0.1 %
PLA/GNP-C 0.25 %
PLA/GNP-C 0.5 %

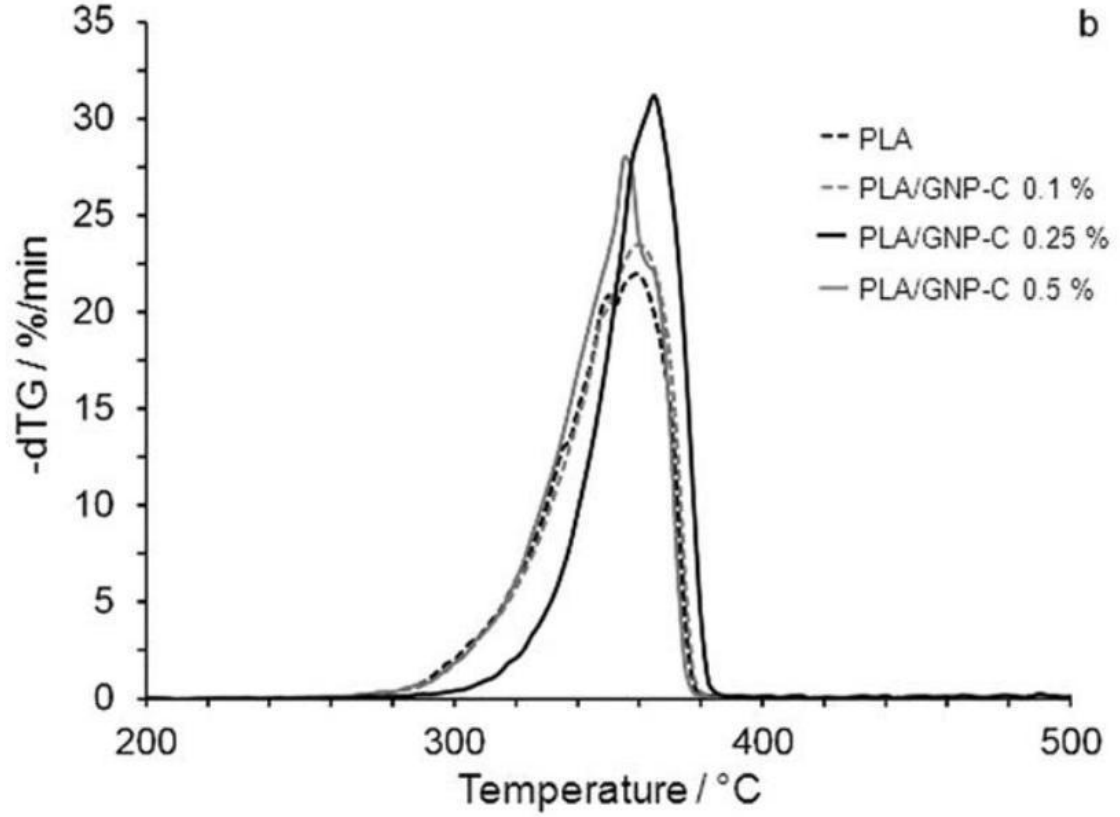
b
35
30
25
20
15
10
5
0
-dTG / %/min
200
300
400
500
Temperature / °C
PLA
PLA/GNP-C 0.1 %
PLA/GNP-C 0.25 %
PLA/GNP-C 0.5 %

FIG. 6. (a) TGA; (b) - dTG curves for PLA and PLA/GNP-C composites with different filler contents (180°C, 20 min, and 50 rpm).

PBS in a 1:80 dilution for 20 min in the dark, to stain cell cytoskeletal filamentous actin. After rinsing with PBS, 4',6-diamidino-2-phenylindole dihydrochloride (DAPI; Sigma-Aldrich) solution at 3μ g mL^{-1} was added to each well and incubated for 15 min in the dark to stain the cell nucleus. Finally, cells were washed and kept in PBS to avoid drying. Plates with adherent cells were observed in an inverted fluorescence microscope (Carl Zeiss - Axiovert 200). For both assays, negative control for toxicity were cells cultured at the surface of PLA incubated in DMEM+, for positive control cells at PLA surface were incubated in DMEM+ with Triton 0.1wt%.

RESULTS AND DISCUSSION

GNP-C Physicochemical Characterization

XPS results (Fig. 1a) show that GNP-C presents a low degree of oxidation (atomic percentage of oxygen, O 1 s = 4%), as expected for a graphene-based material that should present oxygen-containing functional groups mostly at the platelet edges. Thermogravimetry results (Fig. 1b) show that most of the thermal degradation of GNP-C occurs above 450°C, the initial slight decrease in weight being associated with desorption of impurities. About 9% weight decrease is observed between 450 and 800°C, probably due to loss of oxygen-containing groups. In many works, GBM with single or few layers are obtained by exfoliation of graphite through oxidative processes, which lead to obtainment of materials with high oxygen content [40]. On the other hand, GNP-C is exfoliated by rapid microwave heating, followed by ultrasonic treatment; therefore, oxygen content is only associated to structural defects at the edges of basal planes. For comparison, Haubner et al. observed that pristine graphite presents an oxygen content of 1.4% and weight loss below 5% when heated until 800°C [41].

FTIR Analysis

Figure 2 shows the spectra typical for PLA presenting peaks from 3000 to 2850 cm^{-1}, correspondent to alkyl $C-H$ stretches. The $C=O$ stretching region appears around 1750 cm^{-1}. A band at 1450 cm^{-1} attributed to CH_3 is found. The $C-H$ deformation and asymmetric bands are present at 1380 and 1355 cm^{-1}. The $C-O$ stretching modes of the ester groups are present around 1178 cm^{-1}. A band correspondent to $C-O-C$ asymmetric stretching is present around 1078 cm^{-1}, and $C-O$ alkoxy stretching vibration mode is at 1060 cm^{-1}. Also, a band correspondent to $C-CH_3$ vibrations is present around 1041 cm^{-1}. Bands at 865 and 754 cm^{-1} are attributed to the amorphous and crystalline phase of PLA, respectively [42, 43].

FTIR spectra for PLA and PLA/GNP-C 0.25wt% are similar. The low filler content makes it difficult to detect characteristic bands. Kong et al. also observed that incorporation of

small amounts (0.3-3 wt%) of carbon fillers (MWNTs) in the polyester poly(caprolactone) did not change the pristine polymer FTIR spectra [44].

Mechanical Characterization

By adjusting operation parameters in melt blending, one can try to obtain a compromise between maximizing filler exfoliation and minimizing thermal/oxidative PLA degradation. In the literature, typical conditions for PLA melt processing correspond to temperatures of 160180°C, mixing times of 10 – 20 min, and rotation speeds around 50 rpm [3, 34, 45]. In this work, PLA/GNP-C blends were initially prepared by mixing at 180°C during 20 min and at 50 rpm . The resulting composites were characterized in terms of Young's modulus, tensile strength, and toughness (area under stress-strain curve, AUC). Figure 3 shows that Young's modulus and tensile strength are maximum for a loading of 0.25wt%, with 20% increase in tensile strength, 12% increase in Young's modulus, and 16% increase in toughness. In comparison, Chartarrayawadee et al. [46] observed an increase of 32%

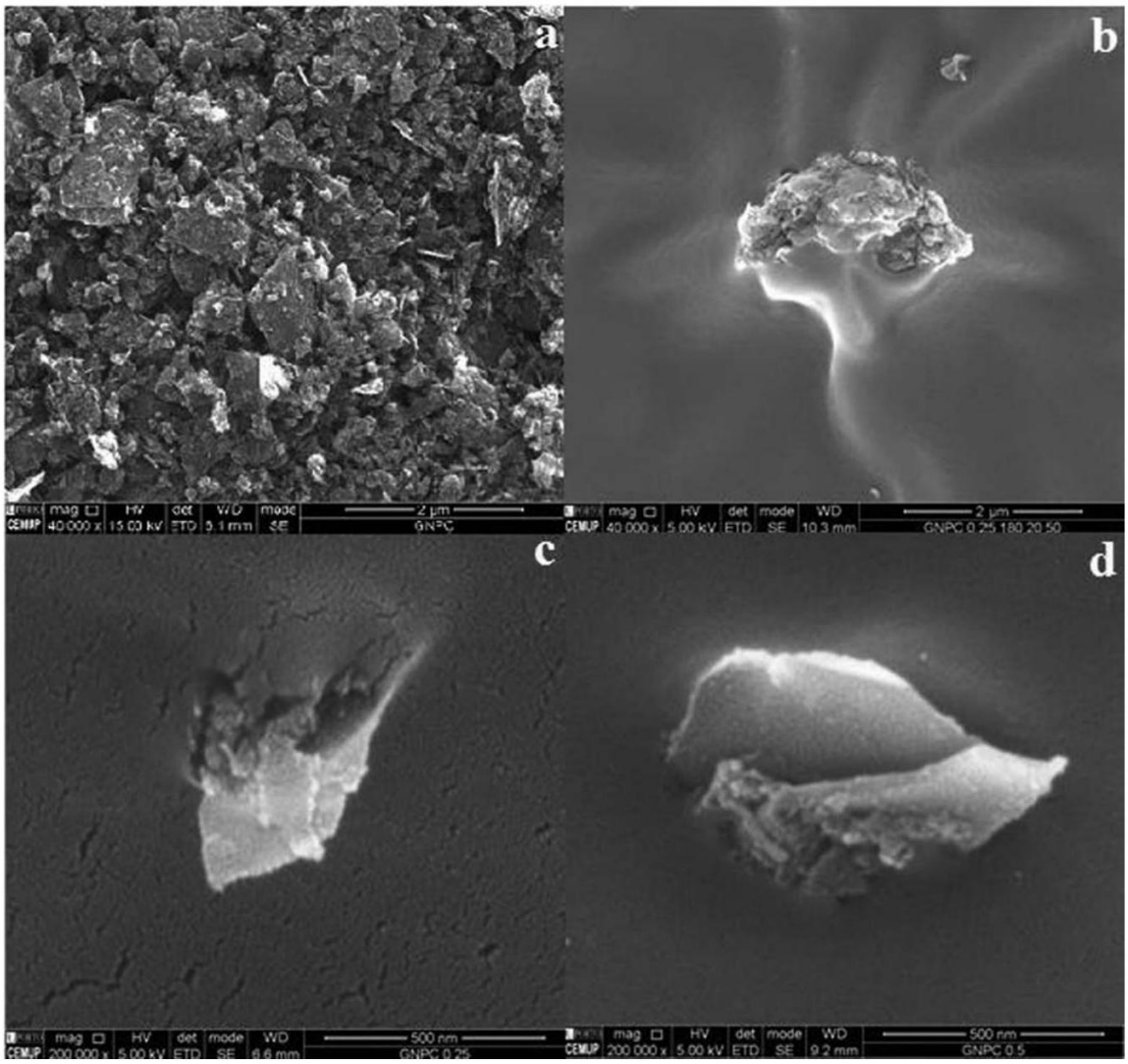

FIG. 7. (a) SEM images of GNP-C powder at 100,000 × magnification; (b) fracture surfaces (under liquid nitrogen) of PLA/GNP-C composites (180°C, 20 min, and 50 rpm), showing GNP-C agglomerates at 40,000 × magnification; (c, d) individualized platelets at 200,000 × magnification, for loadings of 0.25 and 0.5wt% in PLA (180°C, 20 min, and 50 rpm), respectively.

in tensile strength with the incorporation of 1wt% graphene oxide and stearic acid (1:1 ratio) in PLA. Also, Li et al. [47] reported an increase in tensile strength of 39% with the incorporation of 1wt% graphene sheets in PLA. On the other hand, Narimissa et al. [48] observed PLA/ GNP-M 1wt% composites to have similar tensile strength and Young's modulus as pristine PLA, becoming brittle at 3wt% loading.

Figure 3 shows the decrease in mechanical performance when loading is raised to 0.5wt%, which can be attributed to increased platelet agglomeration introducing defects in the polymer matrix. The relation between agglomeration and loading level will be discussed further below. Toughness improves for 0.1 and 0.25wt% loadings, when compared to pristine PLA, but the two results are undistinguishable. Elongation at break results was of about 3.8%, with no significant differences observed between PLA and its composites.

The effects of varying mixing time and rotation speed were analyzed for the optimal loading of 0.25wt%. Figure 4 compares the results obtained for mixing times of 10, 15, and 20 min , and rotation speeds of 25 and 50 rpm . At 75 rpm , a brittle material was obtained, probably due to PLA degradation under high shear. The results show that the best processing conditions correspond to 20 min and 50 rpm . Lower mixing time or rotation speed probably yield worse GNP dispersion and hence lower mechanical performances. A higher mixing temperature of 200°C was tested, but yielded very brittle materials, probably due to thermoxidative degradation of PLA. These results show that tuning of melt blending operation conditions can have an impact on the final properties of the nanocomposite, as it directly affects the quality of nanofiller dispersion and then possibility of polymer degradation.

Since the best processing conditions for PLA and PLA/GNP-C were determined to be 180°C, 20 min, and 50 rpm , only the materials produced using these conditions were further characterized on physicochemical and biological studies.

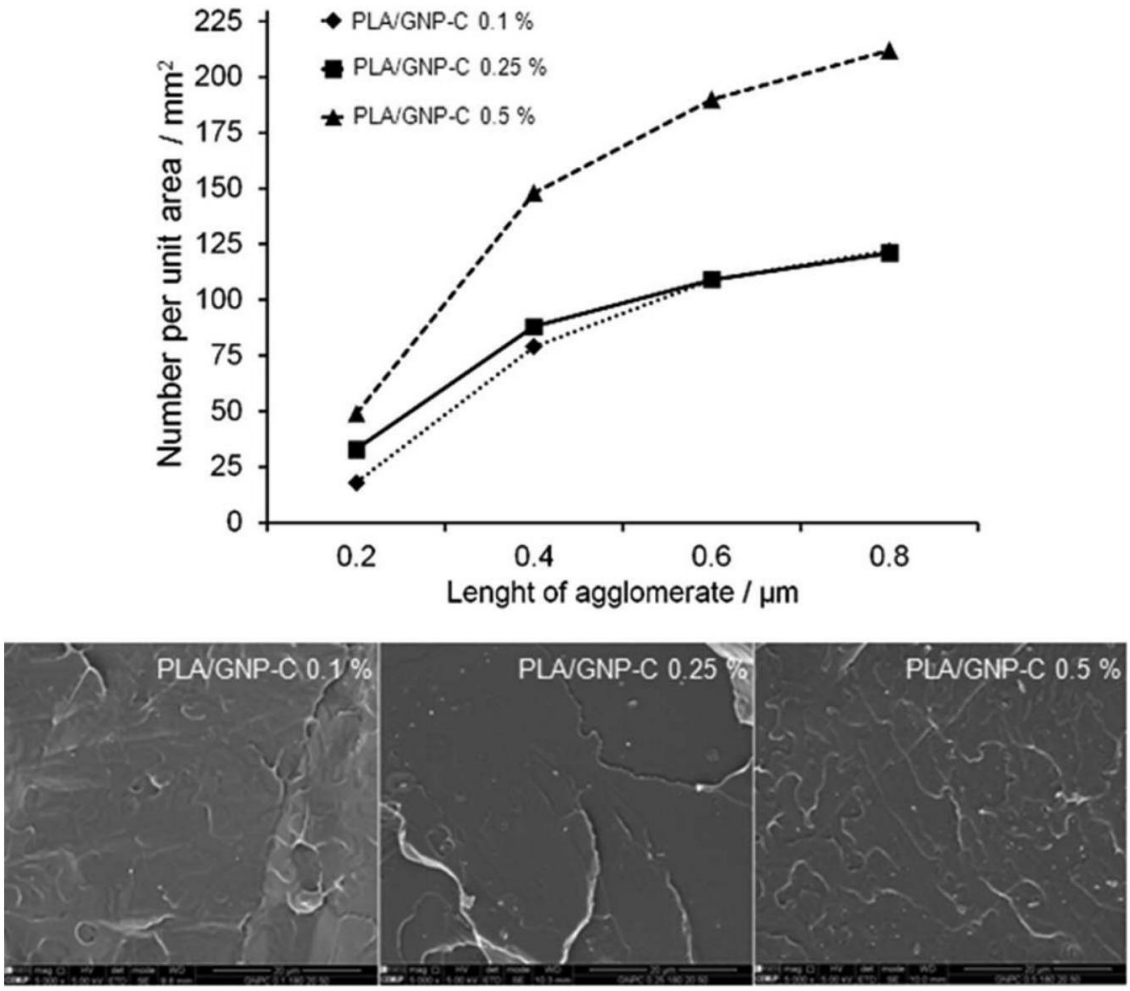

FIG. 8. (a) Cumulative plots of number of agglomerates per unit of area (mm^2) as a function of agglomerate length, for different GNP-C loadings (180°C, 20 min, and 50 rpm); (b) SEM images of fracture of surfaces for 5,000 × magnification.

Thermal Analysis

Differential scanning calorimetry (DSC) was performed for all PLA/GNP-C loadings tested. The results are shown in Fig. 5. Glass transition occurs in the range 60 – 65°C, followed by a small hysteresis peak, associated

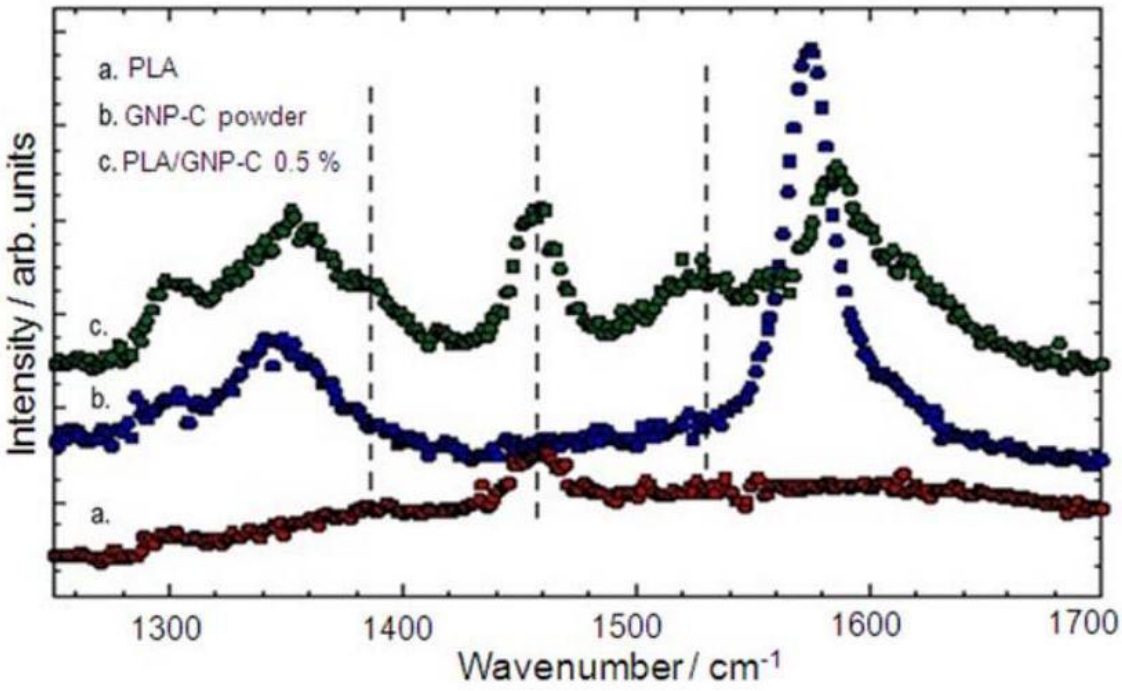

FIG. 9. Representative unpolarized Raman spectra for PLA, GNP-C powder, and PLA/GNP-C 0.5wt%20 min, recorded at ambient conditions with physical relaxation. Melting takes place at around 155°C, preceded by a broad cold-crystallization peak. It is interesting to note that PLA presents two combined melting peaks, which can be ascribed to differences in crystal morphology (e.g., lamellar thickness) [49]. As GNP-C content increases, the higher temperature peak diminishes in intensity, indicating that polymer-nanoplatelet interaction leads to crystallinity uniformization.

Table 1 shows the estimated values of glass transition temperature (T_g) and melting temperature (T_m) for all samples tested. As the material is loaded with GNP-C, both T_g and T_m do not change significantly in relation to pristine PLA. An increase in T_g is often expected as a consequence of segment mobility being restricted due to filler-induced chain confinement. However, other studies have reported similar behavior for PLA loaded with nanofillers, concomitantly with observation of mechanical reinforcement [35, 39]. A decrease in T_m would be observed if phase separation had occurred [50,51].

The computed degree of crystallinity (χ_c) is also shown in Table 1. Crystallinity seems to increase with GNP addition, but the differences are very small and are not expected to have a significant influence on the

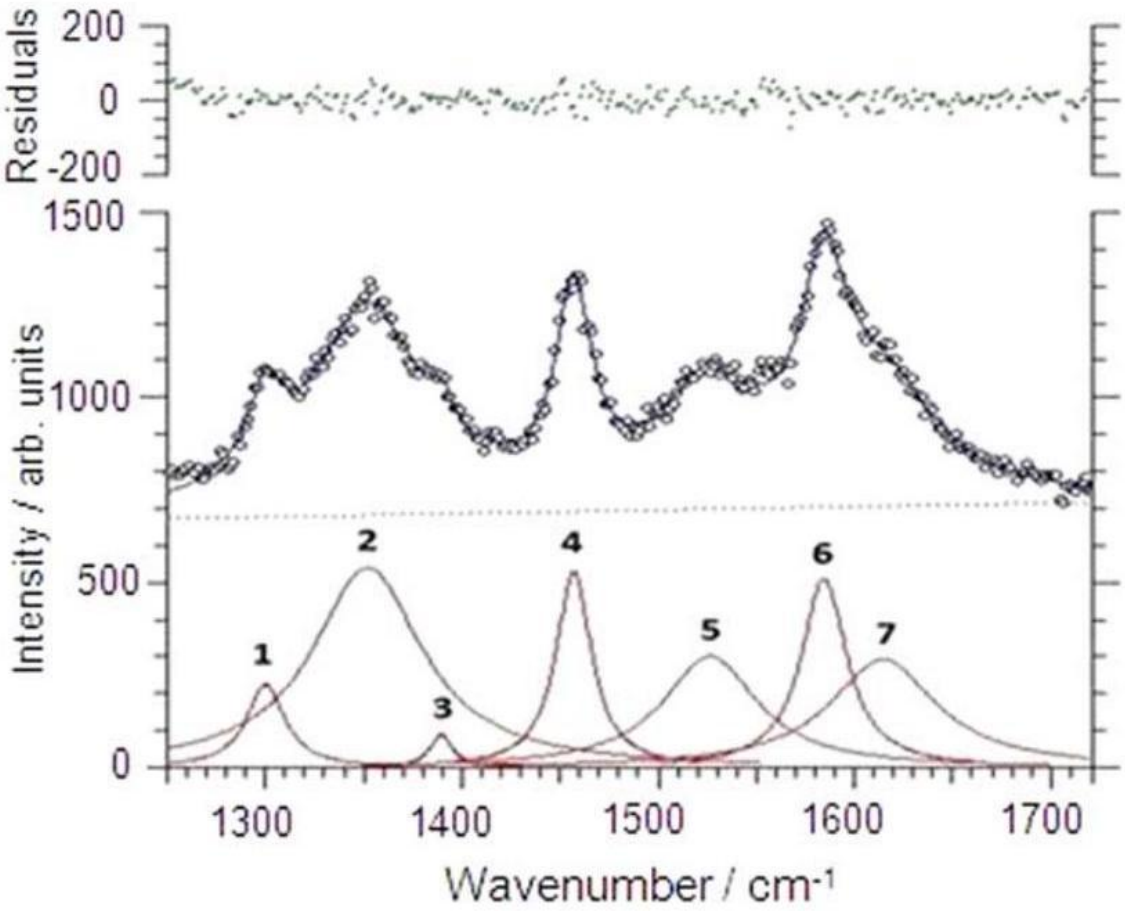

FIG. 10. Example of Raman spectrum fitting according to Eq. 1 to PLA/GNP-C 0.5wt%20 min. Bands 1 – 3 are attributed to D band and 5-6 to G band of GNP-C, while band 4 arises from PLA matrix. [Color figure can be viewed in the online issue, which is available at wiley onlinelibrary.com.]

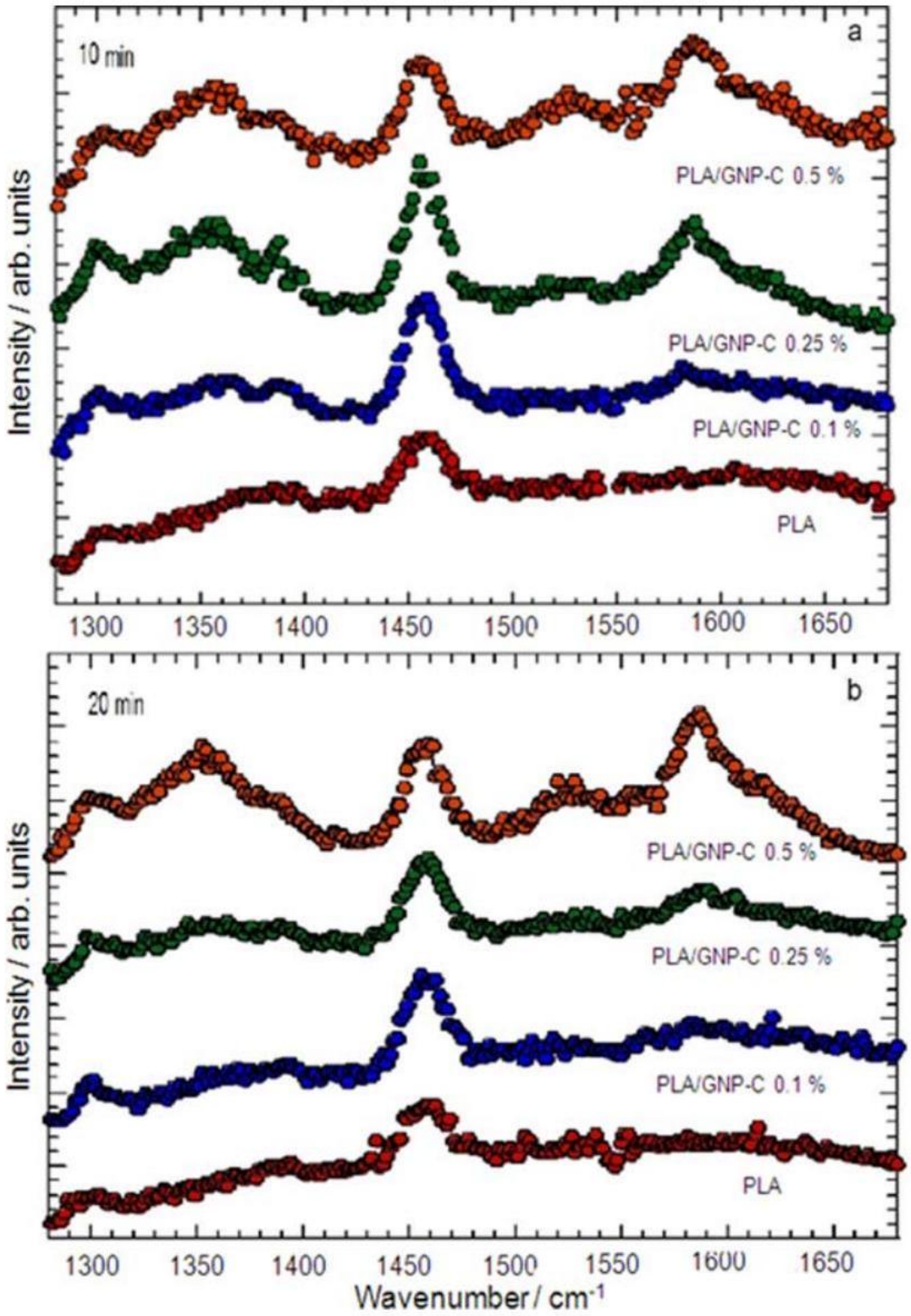

FIG. 11. Unpolarized Raman spectra of PLA and PLA/GNP-C 0.1, 0.25 , and 0.5wt% for (a) 10 and (b) 20 min mixing times.

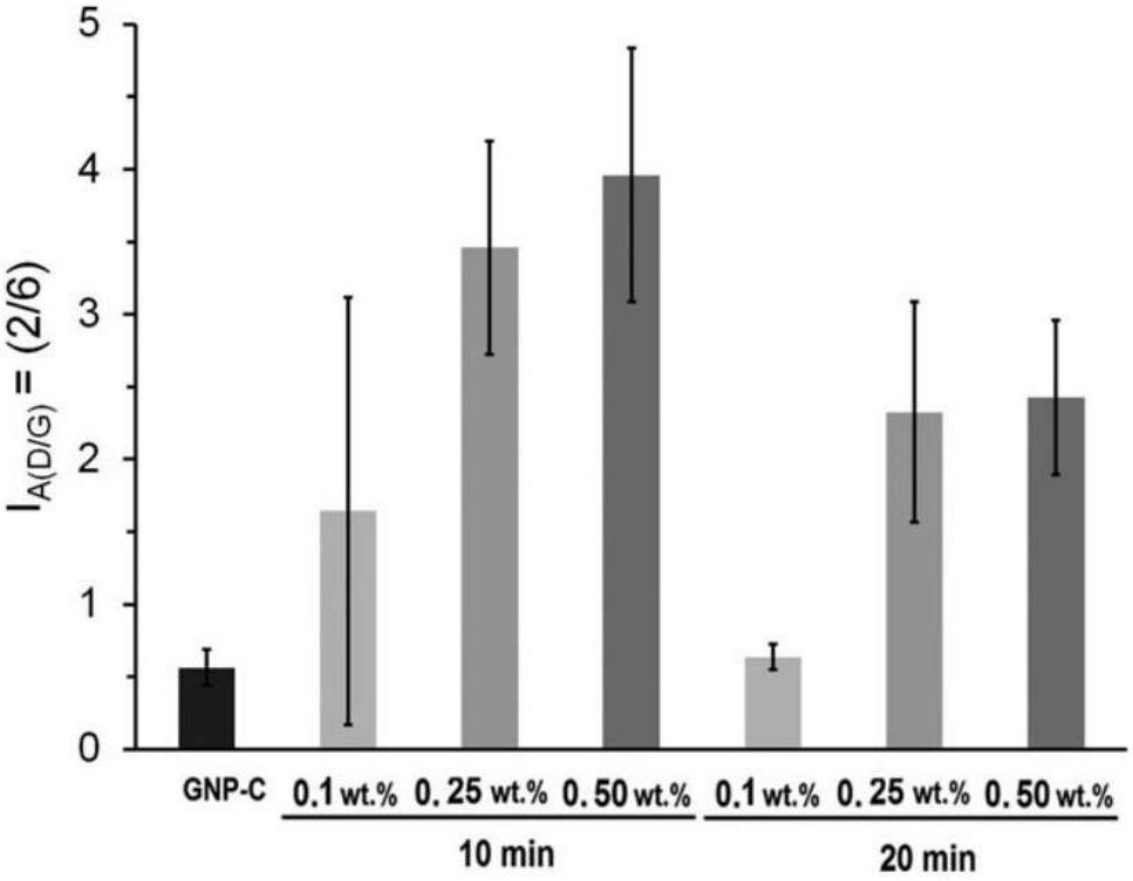

FIG. 12. Intensity ratios of the D and G bands of monolayer GNP-C (peak 2/peak 6) for GNP-C powder and PLA/GNP-C 0.1, 0.2, and 0.5 wt% for 10 and 20 min mixing times. Results are presented as average values and error bars represent standard deviation ($n > 3$).

mechanical properties of the material. Interestingly, for the condition that resulted in better dispersion and mechanical performance (PLA/GNP-C 0.25wt%, 180°C, 20 min , and 50 rpm), T_c is decreased by 3°C, ΔH_c increased by 3 J g^{-1}, and crystallinity increased by 3%. This probably occurs because GNP-C particles cause heterogeneous nucleation, anticipating and increasing crystallization, as proposed by Kong et al. [52] for MWNTs, and similarly observed by Wang et al. [53] for GO.

Figure 6a shows the thermogravimetric curves obtained for pristine PLA and PLA/GNP-C. Thermal degradation is very similar for all samples: a single step between 300°C and 370°C, as expected for PLA [54]. Figure 6b, which represents the weight loss derivative (dTG) curves, allows a better differentiation between the results. The peak maximum values increase with graphene loading, indicating faster degradation rates. Similar behavior has been reported by Bao et al. [35] for PLA/graphene composites, which was attributed to the high thermal conductivity of graphene being the dominant contribution at low loadings. As a consequence, facilitated heat transfer overcomes the mass transfer barrier effect that often leads to improved thermal stabilities when lamellar fillers are used. In our particular case, the relatively small diameter of the GNP-C platelets may contribute to it being a less effective barrier, as the effect of path tortuosity is small. For a loading of 0.5wt%, the onset of degradation is shifted toward higher temperatures, which

may indicate that at this concentration, diffusion of pyrolysis products is more effectively restrained.

Scanning Electron Microscopy

SEM imaging was performed on PLA/GNP-C composites fractured under liquid nitrogen. Figure 7 shows the original GNP-C powder (Fig. 7a) and platelets found in

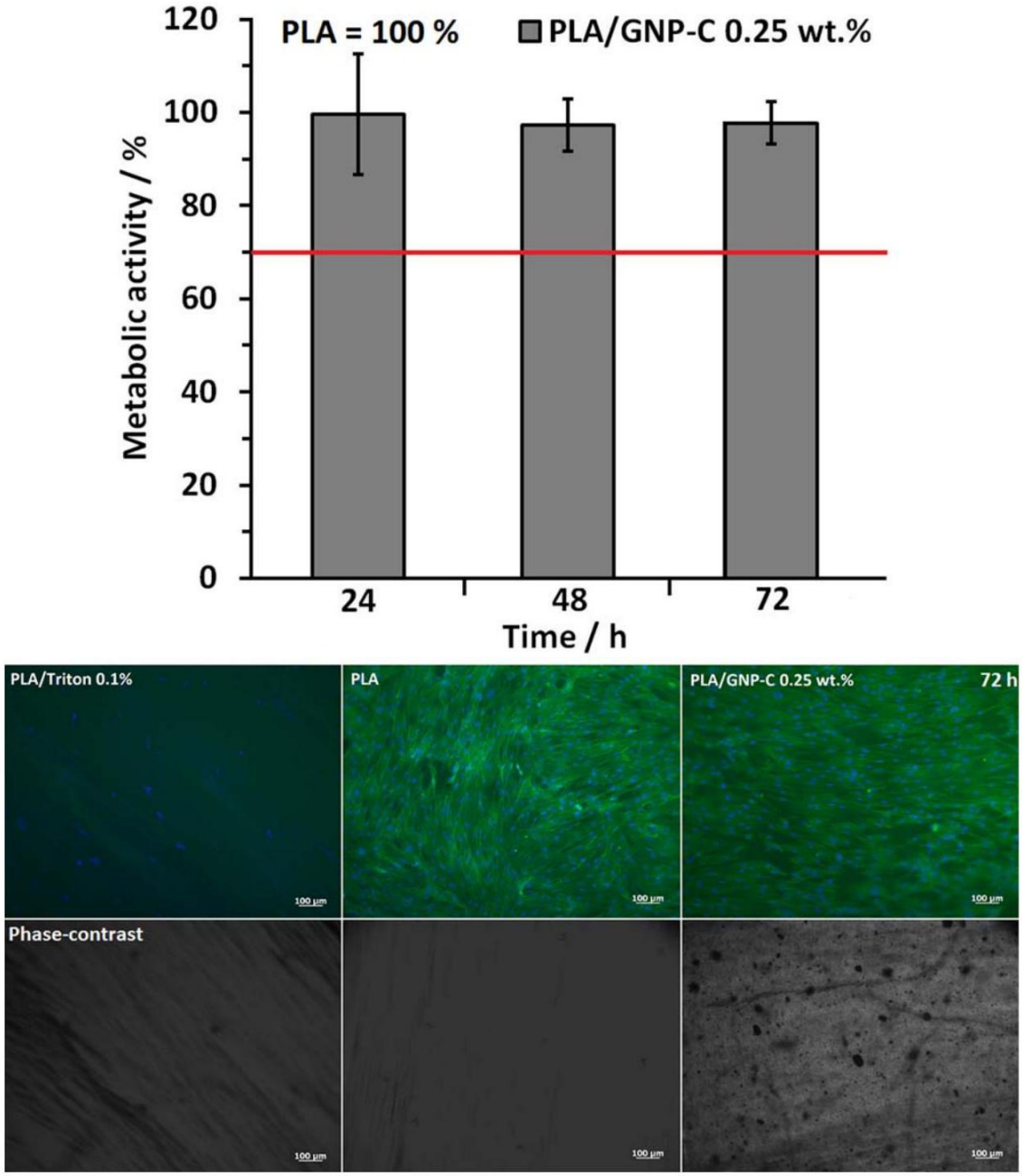

FIG. 13. Metabolic activity of HFF-1 cells cultured at the surface of PLA/GNP-C 0.25wt%(180°C, 20 min , and 50 rpm) in DMEM+, at 24,48 , and 72 h . Cell metabolic

activity is represented as percentage in comparison with cells cultured at PLA surface in DMEM + (100%). Results are presented as mean and standard deviation ($n = 6$). The red line at 70% marks the toxicity limit, according to ISO 10993-5:2009(E). For positive control of cell death, cells were cultured at PLA surface in DMEM+/Triton 0.1%, with metabolic activity being close to 0% (data not shown). For representative immunofluorescence images of HFF-1 at 72 h , cells were stained with DAPI (nuclei) blue and phalloidin (F-actin in cytoskeleton) green. Bottom line presents the phase-contrast images of materials surface. Scale bar represents 100μ mfracture surfaces (Fig. 7b-d). Figure 7a shows that the powder is composed of flat platelets, lower than 2μ m in length, and smaller flake agglomerates. Figure 7b displays one of the largest agglomerates found in the fractured PLA matrix, which is seen to be composed of small aggregated flakes. Planar GNP can also be found embedded in the matrix (Fig. 7c and d), showing that platelet individualization was achieved in the melt dispersion process.

As previously discussed, agglomeration at the higher loadings is the probable cause for the observed degradation of mechanical properties above 0.25wt% GNP-C content. To obtain a better notion of the incidence of agglomeration in these composites, different SEM images of fracture surfaces (at 5,000 × magnification) were inspected, and the number of agglomerates with different average sizes was computed per unit area of sample section, for the three loadings tested. Figure 8 shows the cumulative plots obtained and representative images. Very few agglomerates were found with sizes above 0.8 μm, and therefore these were ignored in the calculations. From Fig. 8, the composites with 0.1 and 0.25wt% loadings show similar results. However, for 0.5wt%, there is a noticeably higher concentration of agglomerates of all sizes. This is consistent with the observed decrease in mechanical performance. At this loading interplatelet interactions promote higher agglomeration, which cannot be efficiently overcome by melt mixing. The agglomerates work as defects in the polymer matrix, facilitating crack initiation during mechanical deformation [55].

Raman Spectroscopy

As observed in Fig. 9, the Raman spectrum of pristine PLA exhibits a well-defined band at 1458 cm^{-1}, in the $1200 - 1700\ cm^{-1}$ spectral range. The Raman spectrum of the "as-received" GNP-C powder exhibits the strong Dand G-bands, located at 1345 cm^{-1} and at 1575 cm^{-1}, respectively, as well as the weak D′-band at 1615 cm^{-1} [56, 57]. The G-band is assigned to the in-plane TO and LO vibrations of the carbon lattice, while the D and D′ bands arise from double resonance processes involving the in-plane TO phonon with defects and edge structure of the graphene sheets. The Raman spectrum of PLA/ GNP-C 0.5wt%, presented here as representative example, exhibits a band at 1458 cm^{-1}, from PLA matrix, and two sets of bands located at the left and right sides of this one, which deserve detailed attention.

Figure 10 shows the best fit of Eq. 1 to the spectrum of PLA/GNP-C 0.5wt%. Both low and high frequency sets can be deconvoluted into three main bands. The existence of several bands in the spectral range where the Dband is expected and where the PLA matrix does not exhibit any Raman band, evidencing structural disorder in the samples due to the exfoliation degree of GNP. In fact, the width of the D bands increases in the composites, evidencing disorder, as reported by Ramirez et al. [56]. The two bands, not presented in pristine GNP-C or PLA matrix spectra, appear in the composite sample: peak 3 at 1390 cm^{-1} and peak 5 at 1525 cm^{-1}. The existence of these bands is an evidence of

physical interaction between polymer matrix and GNP-C, originating new modes in the system. Moreover, the frequency upshifts, of about 5 and 10 cm^{-1} observed for peaks 2 and 6, respectively, when GNP-C is incorporated in PLA, corroborates the fil-ler-matrix interaction and compression of the filler by the polymer matrix upon cooling [58].

Figure 11 shows the representative Raman spectra of PLA and PLA/GNP-C composites with different filler amounts, mixed during 10 (Fig. 11a) and 20 min (Fig. 11b). In both cases, as the graphene concentration increases, the intensity of Raman bands assigned to GNPC increases. The Raman signals recorded for different sample positions did not show significant differences, pointing out the homogeneity of the graphene distribution within the polymer matrix, considering both individualized platelets and agglomerates.

From the fitting procedure, we have calculated the intensity of the observed Raman bands. It is well established that the ratio between the intensities of the D - and G-bands, I_D/I_G, is widely used for characterizing the level of defect in graphene [59]. Moreover, the intensity of a Raman band depends on the scattering cross-section of the corresponding mode and on the number of scatters per unit volume. Therefore, the ratio between the intensities of two aforementioned modes gives qualitative information regarding the ratio between the corresponding scatters concentration [60]. Figure 12 shows the ratio between the intensities relative to the D and G bands (peaks 2 and 6), for the as-received GNP-C powder and to the PLA/GNP-C composites, for 10 and 20 min mixing times. In both cases, as the GNP-C concentration increases, the ratio I_2/I_6 tends to increase, which is interpreted as an evidence for the increasing disorder in graphene, associated with defects arising from the interaction between graphene sheets and the polymeric matrix, and from the agglomerates of graphene in the matrix, as it is well evidenced by the SEM images. For a sufficiently high filler loading (0.5wt%), the content of agglomerated material introduces defects that can have a negative impact on the mechanical performance of the composite. This detrimental action surpasses the reinforcement effect, in agreement with the results of mechanical testing. This interpretation of the I_D/I_G ratio is consistent with the fact that, for the same GNP-C initial concentration, the ratio decreases with increasing mixing time, evidencing that longer mixing induces more efficient deagglomeration of the nanoplatelets within the PLA matrix.

Biocompatibility with Fibroblasts

Biocompatibility was studied by culturing cells at materials' surface, evaluating cell metabolic activity and morphology. For providing a negative control for cell death, cells were cultured at the surface of PLA, presenting the typical "spindle"-like shape of fibroblasts. This was expected, as PLA is generally a biocompatible material [61]. For positive control of cell death, PLA cultured in DMEM+ with Triton 0.1%, metabolic activity was close to 0% and cytoskeleton was disassembled. Since the best mechanical results were obtained for PLA/GNP-C 0.25wt%(180°C, 20 min, and 50 rpm), only these materials were tested on biological assays.

HFF-1 cell metabolic activity at PLA/GNP-C 0.25 wt% surface never decreased below 97%, in comparison with PLA (Fig. 13). Also, immunocytochemistry images show no morphological differences between PLA and PLA/GNP-C 0.25wt%. Thus, filler incorporation has no impact on cell growth at materials surface. The fact that a small amount of GNP-C is used, together with the platelets being well encapsulated in the

polymer may be on the base of the lack of toxicity observed [26]. Yoon et al. [62] observed that the incorporation of 2wt%GO in poly(d, l-lactic-co-glycolic acid) matrix by solvent mixing improved neuronal cell metabolic activity. However, Lahiri et al. [63] observed ultrahigh molecular weight polyethylene/GNP-M 1wt% composites produced by electrostatic spraying to be toxic to osteoblasts. Toxicity can be caused by filler leaching [26], which suggests that electrostatic spraying may not promote effective embedding of GBM in polymer matrix. Solvent mixing and melt blending seem to be more effective in this sense, therefore, avoiding toxicity effects.

CONCLUSIONS

The purpose of this work was to evaluate the mechanical and thermal properties of PLA filled with GNP-C, which presents particularly small platelet diameters and thicknesses. The effects of blending conditions (mixing time, intensity, and temperature) and nanofiller loading on the composite properties were analyzed. Both factors were observed to have a major effect on the material's performance. The best processing conditions were found to be mixing for 20 min at 50 rpm and 180°C. The optimum loading was 0.25wt%, resulting in 20% increase in tensile strength, 12% increase in Young's modulus, and 16% increase in toughness. At higher loadings, defects due to filler agglomeration cause decay in mechanical performance. The higher incidence of agglomeration at 0.5wt% loading was demonstrated by SEM and Raman analysis, in what we believe are novel approaches for the use of these techniques in composite characterization.

Thermal analysis (DSC and TGA) showed no differences in glass transition or degradation temperature between pristine PLA and the composites. However, an increase in rate of thermal degradation with GNP-C loading was identified, which was interpreted in terms of a dominant effect of enhanced heat transfer over mass transfer barrier, in agreement with other reported works.

Melt mixing intensity and duration were found to have an impact on the mechanical properties of PLA/GNP-C composites. Raman spectroscopy analysis, based on intensity ratios of D and G bands, confirmed that longer mixing times yield better dispersion of GNP. Evidence of effective interaction between the nanofiller and the polymer matrix was found in the form of frequency shifts and appearance of new Raman bands.

HFF-1 cells metabolic activity and morphology were not affected by the incorporation of 0.25wt% GNP-C in PLA.

The increased mechanical performance of these composites, achieved at low filler loadings, associated with their biocompatibility, provides interesting perspectives for use in biomaterial applications.

REFERENCES

1. R. Vaia and H. Wagner, Materials, 7, 32 (2004).
2. A.J.R. Lasprilla, G.A.R. Martinez, B.H. Lunelli, A.L. Jardini, and R.M. Filho, Biotechnol. Adv., 30, 321 (2012).
3. B. Chieng, N. Ibrahim, and W. Yunus, Polym. Plast. Technol. Eng., 51, 791 (2012).

4. B.W. Chieng, N.A. Ibrahim, W.M.Z.Y. Yunus, M.Z. Hussein, and V.S.G. Silverajah, Int. J. Mol. Sci., 13, 10920 (2012).
5. I. Armentano, M. Dottori, E. Fortunati, S. Mattiolo, and J.M. Kenny, Polym. Degrad. Stabil., 95, 2126 (2010).
6. B.D. Ratner, A. Hoffman, F. Schoen, and J. Lemons, Biomaterials Science, Academic Press, Boca Raton (1996).
7. L. Cabedo, J. Feijoo, M. Villanueva, and J. Lagarón, Macromol. Symp., 233, 191 (2006).
8. S. Park, M. Todo, K. Arakawa, and E. Koganemaru, Polymer, 47, 1357 (2006).
9. M. Murariu, A. Ferreira, M. Pluta, L. Bonnaud, M. Alexandre, and P. Dubois, Eur. Polym. J., 44, 3842 (2008).
10. S. Tjong, Mater. Sci. Eng., 53, 73 (2006).
11. M. Nosonovsky and B. Bhushan, Mater. Sci. Eng., 58, 162 (2007).
12. A. Dasari, Z. Yu, and Y. Mai, Mater. Sci. Eng., 63, 31 (2009).
13. N. Kotov, Nature, 442, 254 (2006).
14. L. Zhang, Q. Zhao, L. Liu, and Z. Zhang, Small, 6, 537 (2010).
15. K. Yang, S. Zhang, G. Zhang, X. Sun, S. Lee, and Z. Liu, Nano Lett., 10, 3318 (2010).
16. A. Kumari, S. Yadav, and S. Yadav, Colloids Surf. B Biointerf., 75, 1 (2010).
17. H. Bai, L. Chun, and S. Gaoquan, Adv. Mater., 23, 1089 (2011).
18. M. Pumera, Chem. Record, 9, 211 (2009).
19. M. Kalbaconva, A. Broz, J. Kong, and K. Martin, Carbon, 48, 4323 (2010).
20. Y. Wang, Z. Li, and Y. Lin, Trends Biotechnol., 29, 205 (2011).
21. X. Zhang, J. Yin, C. Peng, W. Hu, Z. Zhua, W. Li, C. Fan, and Q. Huang, Carbon, 49, 986 (2011).
22. Y. Chang, S. Yang, J. Liu, E. Dong, Y. Wang, A. Cao, Y. Liu, and H. Wang, Toxicol. Lett., 200, 201 (2011).
23. P. Begun, R. Ikhtiari, and B. Fugetsu, Carbon, 49, 3907 (2011).
24. D. Lahiri, R. Dua, C. Zhang, I. Socarraz-Novoa, A. Bhat, S. Ramaswammy, and A. Agarwal, ACS Appl. Mater. Interf., 4, 2234 (2012).
25. J. Wang, P. Sun, Y. Bao, J. Liu, and L. An, Toxicol. in Vitro, 25, 242 (2011).
26. A. Pinto, I. Gonçalves, and F. Magalhães, Colloids Surf. B Biointerf., 111, 188 (2013).
27. A.M. Pinto, C. Gonçalves, D.M. Sousa, A.R. Ferreira, J.A. Moreira, I.C. Gonçalves, and F.D. Magalhães, Carbon, 99, 318 (2015).
28. Y. Pan, T. Wu, H. Bao, and L. Li, Carbohydr. Polym., 83, 1908 (2011).
29. P. Song, Z. Cao, Y. Cai, L. Zhao, Z. Fang, and S. Fu, Polymer, 52, 4001 (2011).
30. Y. Cao and P. Wu, Carbon, 48, 3834 (2010).

31. A. Pinto, J. Cabral, D. Tanaka, A. Mendes, and F. Magalhães, Polym. Int., 62, 33 (2012).

32. X. Li, Y. Xiao, A. Berget, M. Longery, and J. Che, Polym. Compos., 35, 396 (2013).

33. A. Pinto, S. Moreira, I. Gonçalves, A. Mendes, and F. Magalhães, Colloids Surf. B Biointerf., 104, 229 (2013).

34. B. Chieng, N. Ibrahim, W. Yunus, and M. Hussein, Polymers, 6, 93 (2014).

35. C. Bao, L. Song, W. Xing, B. Yuan, C. Wilkie, J. Huang, Y. Guo, and Y. Hu, J. Mater. Chem., 22, 6088 (2012).

36. J.H. Yang, S.H. Lin, and Y.D. Lee, J. Mater. Chem., 22, 10805 (2012).

37. I. Kim and Y.G. Jeong, J. Polym. Sci. B: Polym. Phys., 48, 850 (2010).

38. L. Wenxiao, S. Chengbo, S. Mingjing, G. Qiwei, X. Zhiwei, W. Zhen, Y. Cauyun, M. Wei, and N. Jiarong, J. Appl. Polym. Sci., 130, 1194 (2013).

39. L. Wenxiao, X. Zhiwei, C. Lei, S. Mingjing, T. Xu, Y. Caiyun, L. Hanming, and Q. Xiaoming, Chem. Eng. J., 237, 291 (2014).

40. K. Loh, Q. Bao, P. Ang, and J. Yang, J. Mater. Chem., 20, 2277 (2010).

41. K. Haubner, J. Morawski, P. Olk, L. Eng, C. Ziegler, B. Adolphi, and E. Jaehne, ChemPhysChem, 10, 2131 (2010).

42. R. Auras, L. Lim, S. Selke, and H. Tsuji, Poly(Lactic Acid): Synthesis, Structures, Properties, Processing, and Applications, John Wiley & Sons (2010).

43. C. Bilbao-Sainz, B. Chiou, D. Valenzuela-Medina, W. Du, K. Gregorski, T. Williams, D. Wood, G. Glenn, and W. Orts, Eur. Polym. J., 54, 1 (2014).

44. Y. Kong, J. Yuan, Z. Wang, and J. Qju, Polym. Compos., 33, 1613 (2012).

45. Z. Antar, J. Feller, H. Noel, P. Glouannec, and K. Elleuch, Mater. Lett., 67, 210 (2012).

46. W. Chartarrayawadee, R. Molloy, A. Ratchawet, N. Janmee, M. Butsamran, and K. Panpai, Polym. Compos., (2015). Article in press. DOI: 10.1002/pc. 23809.

47. X. Li, Y. Xiao, A. Bergeret, M. Longerey, and J. Che, Polym. Compos., 35, 396 (2014).

48. E. Narimissa, R.K. Gupta, H.J. Choi, N. Kao, and M. Jollands, Polym. Compos., 33, 1505 (2012).

49. T. Liu and J. Petermann, Polymer, 42, 6453 (2001).

50. C. Wu and H. Liao, Polymer, 48, 4449 (2007).

51. M. Murariu, L. Bonnaud, P. Yoann, G. Fontaine, S. Bourbigot, and P. Dubois, Polym. Degrad. Stabil., 95, 374 (2010).

52. Y. Kong, J. Yuan, Z. Wang, and J. Qiu, Polym. Compos., 33, 1613 (2012).

53. H. Wang and Z. Qiu, Thermochim. Acta, 526, 229 (2011).

54. K. Das, D. Ray, I. Baneriee, N. Bandyopadhyay, S. Sengupta, A.K. Mohanty, and M. Misra, J. Appl. Polym. Sci., 18, 143 (2010).

55. Tjon, S, Nanocrystalline Materials: Their Synthesis-Struc-ture-Property and Applications, 2nd ed., Elsevier, London (2014) 364.

56. C. Ramirez and I. Osendi, J. Eur. Ceram. Soc., 33, 471 (2013).

57. M. Pimenta, G. Dresselhaus, M.S. Dresselhaus, L.G. Cançado, A. Jorio, and R. Saito, Phys. Chem., 9, 1276 (2007).

58. A.C. Ferrari, J.C. Meyer, V. Scardaci, C. Casiraghi, M. Lazzeri, F. Mauri, S. Piscanec, D. Jiang, K.S. Novoselov, S. Roth, and A.K. Geim, Phys. Rev. Lett., 97, 187401 (2006).

59. M. Lucchese, F. Stavale, E.H. Martins, C. Vilani, C.V. Moutinho, B.C. Rodrigo, A.C. Achete, and A. Jorio, Carbon, 48, 1592 (2010).

60. W. Weber, R. Merlin, Raman Scattering in Materials Science, Springer, Berlin (2000).

61. J.M. Anderson and M.S. Shive, Adv. Drug Deliv. Rev., 28, 1 (1997).

62. O.J. Yoon, C.Y. Jung, I.Y. Sohn, H.J. Kim, B. Hong, M.S. Jhon, and N. Lee, Compos. A, 42, 1978 (2011).

63. D. Lahiri, R. Dua, C. Zhang, I. Socarraz-Novoa, A. Bhat, S. Ramaswamy, and A. Agarwal, ACS Appl. Mater. Interf., 4, 2234 (2012).

64. K. Kalaitzudou, H. Fukushima, and L. Drzal, Compos. A, 38, 1675 (2007).

65. E. Fischer and H. Sterzel, Polymer, 251, 980 (1973).

66. A. Moreira, A. Almeida, M.R. Chaves, M.L. Santos, P.P. Alferes, and I. Gregora, Phys. Rev. B, 76, 174102 (2007).